Master's thesis

Assessing the Patellar Tracking Pattern before versus after Total Knee Arthroplasty using Dynamic Computed Tomography: a Cadaveric Study

Anne van den Brekel, BSc
s1733141

University of Twente
Faculty of Science and Technology
Master's programme: Technical Medicine
Master track: Medical Imaging & Interventions

Radboud university medical center
Department of Orthopaedic Surgery
Orthopaedic Research Lab

Examination Committee
Chairman: Prof. dr. ir. C.H. Slump
Medical supervisor: Dr. ing. S.A.W. van de Groes
Technological supervisor UT: Prof. dr. ir. C.H. Slump
Technological supervisor Radboudumc: Ir. H. Dunning
Process supervisor: Dr. M. Groenier
External member UT: Dr. E. Groot Jebbink

June 28, 2021

Radboudumc

UNIVERSITY OF TWENTE.

Abstract

Purpose: Up to 30% of patients experience anterior knee pain after Total Knee Arthroplasty (TKA). It is thought that a change in the patellar tracking pattern after TKA might lead to anterior knee pain. To clarify this relationship, there is need for a technique to directly assess the patellar tracking pattern before versus after TKA. This study investigated to what extent dynamic Computed Tomography (CT) can be used to assess the patellar tracking pattern before versus after TKA.

Materials and methods: Static and dynamic CT images with different acquisition and reconstruction parameters were obtained of two human cadaveric knees before and after TKA. Qualitative and quantitative image analysis and radiation dose calculations were performed to find the most suitable dynamic CT imaging method. The patellar tracking pattern before and after TKA was assessed from these dynamic CT images in terms of patellar flexion, tilt, rotation and shift.

Results: CT images obtained at the highest tube voltage and tube current, reconstructed without a metal artifact reduction algorithm and with a bone reconstruction kernel provided the best image quality. These images were used to assess the patellar tracking pattern. With the developed method, differences were found between the pre and post TKA patellar tracking pattern.

Conclusion: A method for the assessment of the patellar tracking pattern before versus after TKA using dynamic CT was successfully developed. Once automated, the developed method can be used to clarify the relationship between a change in the patellar tracking pattern after TKA and anterior knee pain. This may potentially guide orthopaedic surgeons in their surgical approach, ultimately improving TKA outcomes.

Keywords: Anterior knee pain, Total knee arthroscopy, Patellar tracking pattern, Computed tomography, Dynamic imaging

Preface

Before you lies my master's thesis "Assessing the Patellar Tracking Pattern before versus after Total Knee Arthroplasty using Dynamic Computed Tomography: a Cadaveric Study". It has been written to fulfill the graduation requirements of the master's programme Technical Medicine at the University of Twente. I was engaged in researching and writing this thesis from September 2020 to June 2021. This thesis was part of my graduation internship, that I conducted at the Department of Orthopaedic Surgery and the Orthopaedic Research Lab of the Radboud university medical center.

In August 2015, I moved all the way from Tilburg to Enschede to study technical medicine, as I was attracted to the idea of improving healthcare with technology. I had a good time in Enschede, where I met a lot of new people and made new friends. Nevertheless, Enschede never really felt like my home. Therefore, after finishing the first year of the master's programme in 2019, I moved to Nijmegen for the clinical internships. In Nijmegen, and certainly in the Radboud university medical center, I did feel at home. Moreover, my interest in the orthopedic profession had been aroused during a short internship in the second year of the master's programme. Therefore, I decided to do my final graduation internship here at the Department of Orthopaedic Surgery.

This thesis officially marks the end of my time as a student. Over the past six years, I have learned a lot of exciting new things. Not only about technical-medical subjects, but also about myself as a person. I am now aware of my skills and qualities and I gained self-confidence. Although the past six years were not always easy, I managed to stay motivated and determined. My hard work is now finally being paid off. I am proud of myself and of what I have achieved and I am looking forward to what the future holds.

I would like to thank my supervisors for their excellent guidance and support during this process. Sebastiaan, I would like to thank you for your feedback from a medical point of view and for giving me the opportunity to develop myself both clinically and personally. Hans, thank you for always finding the time to answer my questions and for steering me in the right direction when I got stuck. Kees Slump, thank you for the valuable input during our online meetings and for the (often humorous) feedback on my writing, where you noticed even the smallest detail. Marleen, thank you for letting me learn a lot about myself and for providing me with new insights that helped me in my personal development. Erik, thank you for joining the graduation committee as the external member. Also huge thanks to the clinical staff and residents of the Department of Orthopaedic Surgery and to the researchers and fellow students of the Orthopaedic Research Lab. And last but not least, I would like to thank my parents Twan and Simone, my sister Lisa, and my boyfriend Mathijs for their support and for always believing in me.

I hope you enjoy reading.

Anne van den Brekel

Nijmegen, June 28, 2021

Table of Contents

1. Introduction 1
1.1. Research questions and thesis outline 3
2. Materials and methods 5
2.1. Data acquisition 5
2.2. Search for suitable dynamic CT imaging method 7
2.2.1. Qualitative image analysis 7
2.2.2. Quantitative image analysis 8
2.2.3. Effective dose calculation 8
2.3. Assessing the patellar tracking pattern 9
2.3.1. Segmentation 9
2.3.2. Registration 9
2.3.3. Patellar motion analysis 10
3. Results 13
3.1. Search for suitable dynamic CT imaging method 13
3.1.1. Qualitative image analysis 13
3.1.2. Quantitative image analysis 14
3.1.3. Effective dose calculation 14
3.2. Assessing the patellar tracking pattern 17
4. Discussion 19
5. Conclusion 25
References 27
Appendix 1: Design space exploration for assessing the patellar tracking pattern 31
Segmentation 31
Registration 31
Patellar motion analysis 32
Appendix 2: Qualitative and quantitative image analysis results 33
Appendix 3: Cadaveric patellar tracking pattern pre versus post TKA 35
Appendix 4: Transform parameter file for binary mask registration 37
Appendix 5: Transform parameter file for image registration 39

1. Introduction

Knee osteoarthritis (OA) is a leading cause of global disability. The global prevalence of radiographically confirmed symptomatic knee OA is 3.8%. [1] Total Knee Arthroplasty (TKA) is an effective and worldwide accepted treatment for severe knee OA, relieving pain and improving knee function [2]. However, up to 30% of patients experience anterior knee pain after TKA [3]. In 2019, 25,859 TKA surgeries and 3,069 knee revision surgeries were registered in the Netherlands. Patellar pain was the reason for revision in 20.2% of patients who underwent knee revision surgery. [4] With the rising number of revision surgeries after TKA in many countries, the financial burden on the healthcare system due to pain is increasing rapidly [5].

The underlying pathology of anterior knee pain following TKA is not yet fully understood [6,7]. It is, however, thought that a change in the patellar tracking pattern after TKA might lead to anterior knee pain [5,6]. The patellar tracking pattern refers to the dynamic relationship between the patella and femoral trochlea during knee movement [8]. Cadaveric studies showed that TKA significantly changes the patellar tracking pattern [9]. The postoperative patellar tracking pattern is influenced by several factors, including the positioning, sizing and design of the (tibial, femoral and optionally patellar) components, but also by surgical soft tissue releases and the formation of scar tissue [5,10].

To clarify the relationship between a change in the patellar tracking pattern after TKA and anterior knee pain, there is need for a technique to directly assess the patellar tracking pattern before versus after TKA. Current techniques are unsatisfactory, as they are either subjective (e.g. the intraoperative 'no thumb technique' [11]) or static (e.g. based on the position of the patella on conventional radiography or Computed Tomography (CT) images) [12]. Therefore, the first aim of this study is to develop a technique to dynamically assess the patellar tracking pattern before versus after TKA. Once this technique has been developed, the relationship between (a change in) the patellar tracking pattern and anterior knee pain can be addressed in a clinical study. Insight in how the patellar tracking pattern might contribute to anterior knee pain could potentially guide orthopaedic surgeons in their surgical approach, ultimately improving TKA outcomes and preventing revision surgeries.

To dynamically assess the patellar tracking pattern, a CT scan with multiple repeated acquisitions during active knee flexion and extension would be preferable [12]. However, there is no standard protocol for the dynamic imaging of a knee after TKA with CT. In addition, usage of CT after TKA is limited by artifacts that appear due to the metallic implant components. Typically, metal artifacts are visible as dark and bright streaks in the vicinity of the metallic objects, resulting in a loss of anatomic detail [13]. Metal artifacts are caused by multiple mechanisms, including beam hardening, Compton scatter, Poisson noise, photon starvation and edge effects [13,14]. These mechanisms corrupt the projection data behind the metal, resulting in a wrong representation of the tissue when reconstructing an image. Metal artifacts are especially noticeable with high density and high atomic number metals [14]. Consequently, the implant material influences the presence of metal artifacts. In addition to metal artifacts, motion artifacts can occur as well, especially with dynamic CT imaging. Motion causes blurring and double

images, as well as long range streaks, thereby lowering the temporal resolution of the CT images [13].
CT acquisition, reconstruction and visualization parameters can be adjusted to improve image quality and reduce metal artifacts. Increasing the x-ray tube voltage and tube current, both acquisition parameters, are classic examples to reduce metal artifacts. Furthermore, the use of a soft tissue reconstruction kernel instead of a bone reconstruction kernel reduces the visibility of the metal artifacts. In addition, the corrupted projection data can be identified and replaced by Metal Artifact Reduction (MAR) algorithms. However, the proposed methods all have their downsides. For example, scanning at a higher tube voltage and tube current increases the radiation dose, while a soft tissue kernel reduces the spatial resolution, and MAR algorithms can create new artifacts. Finally, the material of the metal implant can also influence the presence of metal artifacts. [14]
For the dynamic assessment of the patellar tracking pattern, a good visibility of the bones (especially the patella) and implant components (in particular the femoral component) is essential, while keeping the radiation dose As Low As Reasonably Achievable (ALARA). The second aim of this study is to find a method to dynamically image a knee after TKA with CT that meets these requirements. Accordingly, the influence of CT imaging parameters (i.e. tube voltage, tube current and reconstruction technique) on image quality (i.e. visibility of bones and implant components and presence of metal and motion artifacts) will be investigated. Additionally, it will be examined whether the material of the implant (cobalt-chromium versus oxidized zirconium) influences image quality. Finally, it will be investigated how tube voltage and tube current influence the radiation dose.

1.1. Research questions and thesis outline

The main question of this research is as follows: To what extent can dynamic CT be used to assess the patellar tracking pattern before versus after TKA? To answer this research question, this thesis is divided into two parts. The first part will focus on finding a suitable method (i.e. meeting the requirements of a good visibility of the bones and implant components while keeping the radiation dose ALARA) to image a knee after TKA with dynamic CT. Sub-questions that will be answered in the first part, are:

1. What is the influence of tube voltage, tube current and reconstruction technique on the visibility of the bones and implant components and on the presence of metal and motion artifacts when dynamically imaging a knee after TKA?
2. To what extent does the material of the implant (cobalt-chromium versus oxidized zirconium) influence the visibility of the bones and implant components and the presence of metal and motion artifacts when dynamically imaging a knee after TKA?
3. What is the influence of tube voltage and tube current on radiation dose when dynamically imaging a knee after TKA?

The second part of this thesis will concentrate on developing a technique to assess the patellar tracking pattern before versus after TKA from dynamic CT data. The following sub-questions will be answered in the second part:

4. What are the positions of the metal implants and bones from the dynamic CT data of a knee before and after TKA?
5. What is the patellar tracking pattern in terms of patellar flexion, tilt, rotation and shift before and after TKA?
6. Is there a difference in the patellar tracking pattern before versus after TKA?

2. Materials and methods

The materials and methods section first describes how the data was obtained. Subsequently, the method for finding a suitable dynamic CT imaging method is described. Finally, it is described how the patellar tracking pattern was assessed from the dynamic CT data.

2.1. Data acquisition

Two fresh-frozen human cadaveric right knees were implanted with a bi-cruciate stabilizing total knee system (Journey II BCS, Smith & Nephew, Watford, England, United Kingdom) by an orthopeadic surgeon with 10 years of experience (Figure 1a). Of the available implants, the first cadaveric knee received a left cobalt-chromium (CoCr) femoral component and the second cadaveric knee received a right oxidized zirconium (Zr) femoral component (Figure 1b). The size of the femoral components was identical. Both cadaveric knees did not receive a patellar component. Pre TKA static and dynamic CT data of the cadaveric knee with the CoCr femoral component was available. Post TKA static and dynamic CT data of both cadaveric knees were obtained. CT imaging was performed with the Aquilion ONE PRISM Edition (Canon Medical Systems Corporation, Otawara, Tochigi, Japan). For static CT imaging, the cadaveric knees were placed in extension on the scanner table. For dynamic CT imaging, the proximal femur was fixated at the end of the scanner table, with the tibia hanging over the edge of the table. A wooden stick was attached to the distal tibia. While scanning, the cadaveric knee was flexed and extended by one of the researchers via the wooden stick (Figure 1c). A total of 41 CT scans were obtained in 10 seconds, providing a frame rate of 4.1 s^{-1}. Each dynamic CT data set thus comprised of 41 CT scans at different knee flexion angles, referred to as dynamic CT frames.

CT imaging parameters (tube voltage in kilovolts (kV), tube current in milliamperes (mA), exposure time in milliseconds (ms), exposure in milliampere-seconds (mAs), slice thickness in millimeter (mm) and pixel spacing (similar row and column spacing) in mm) of the pre TKA static and dynamic CT data are shown in Table 1. These pre TKA imaging parameters were in accordance with the imaging parameters that are used in our institution for scanning knees without metal implants. Pre TKA static CT scans were obtained with a tube voltage of 100 kV and an exposure of 10 mAs. A bone kernel was used for image reconstruction. Pre TKA dynamic CT frames were obtained with a tube voltage of 100 kV and an exposure of 7 mAs. A soft tissue kernel was used for image reconstruction. CT imaging parameters of the post TKA static and dynamic CT data are shown in Table 2. As for the pre TKA static CT scans, post TKA static CT scans were obtained with a tube voltage of 100 kV and an exposure of 10 mAs. In addition, post TKA static CT scans with a tube voltage of 120 kV and an exposure of 40 and 150 mAs were obtained. As for the pre TKA dynamic CT frames, post TKA dynamic CT frames were obtained with a tube voltage of 100 kV and an exposure of 7 mAs. Additional post TKA dynamic CT frames with a tube voltage of 120 kV and an exposure of 17 mAs were obtained. Post TKA static CT scans and dynamic CT frames were reconstructed with both a soft tissue and a bone kernel and both with and without the Single Energy Metal Artifact

Reduction (SEMAR) [15] algorithm. This resulted in a total of 16 static CT reconstructions and 12 dynamic CT reconstruction sets post TKA.

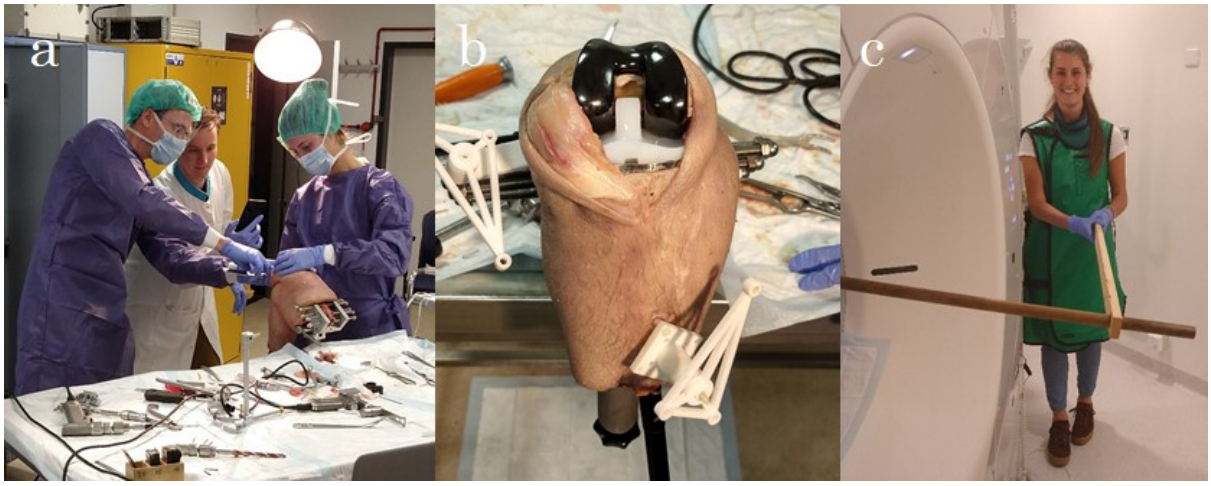

Figure 1: a) Implantation of a total knee system in a cadaveric knee. b) Cadaveric knee with a total knee system. c) Flexion and extension of the cadaveric knee in the CT scanner via a wooden stick construction.

Table 1: CT imaging parameters (tube voltage in kilovolts (kV), tube current in milliamperes (mA), exposure time in milliseconds (ms), exposure in milliampere-seconds (mAs), slice thickness in millimeter (mm) and pixel spacing (similar row and column spacing) in mm) of the pre TKA static and dynamic CT data.

	Tube voltage (kV)	Tube current (mA)	Exposure time (ms)	Exposure (mAs)	Slice thickness (mm)	Pixel spacing (mm)
Pre TKA static	100	20	500	10	1.0	0.44
Pre TKA dynamic	100	40	175	7	0.5	0.98

Table 2: CT imaging parameters (tube voltage in kilovolts (kV), tube current in milliamperes (mA), exposure time in milliseconds (ms), exposure in milliampere-seconds (mAs), slice thickness in millimeter (mm) and pixel spacing (similar row and column spacing) in mm) of the post TKA static and dynamic CT data.

	Tube voltage (kV)	Tube current (mA)	Exposure time (ms)	Exposure (mAs)	Slice thickness (mm)	Pixel spacing (mm)
Post TKA static	100	20	500	10	0.5	0.40
	120	20	500	10	0.5	0.40
	120	80	500	40	0.5	0.40
	120	300	500	150	0.5	0.40
Post TKA dynamic	100	40	175	7	0.5	0.98
	120	40	175	7	0.5	0.98
	120	100	175	17	0.5	0.98

2.2. Search for suitable dynamic CT imaging method

The aim was to find a suitable method (i.e. good visibility of the bones and implant components while keeping the radiation dose ALARA) to image a knee with dynamic CT after TKA. Accordingly, a qualitative image analysis of the post TKA static CT reconstructions and dynamic CT reconstruction sets was executed first. Second, a quantitative image analysis of the post TKA static CT reconstructions was performed. Third, a calculation of the effective dose of the static CT scans and dynamic CT data sets was executed.

2.2.1. Qualitative image analysis

The influence of tube voltage, tube current and reconstruction technique on the visibility of the bones and implant components and on the presence of metal and motion artifacts was investigated by qualitative assessment of the post TKA static CT reconstructions and dynamic CT reconstruction sets of the knee with the CoCr implant. The presence of metal and motion artifacts and the visibility of the patella, femoral condyles, proximal tibia, femoral component and tibial component were rated on a five-point Likert scale (Table 3). Rating was performed by an orthopaedic surgeon with 10 years of experience and a radiologist with 3 years of experience in musculoskeletal radiology, who reached a consensus. Static CT reconstructions were visualized with 3D Slicer (version 4.10.2) [16] and dynamic CT reconstruction sets were visualized with VV Viewer (version 1.4) [17]. All reconstructions were displayed in a bone window (i.e. window width of 1800 Hounsfield Units (HU) and window level of 400 HU).

Similarly, the influence of the implant material on the visibility of the bones and implant components and the presence of metal and motion artifacts was investigated. The presence of metal and motion artifacts and the visibility of the patella, femoral condyles and femoral component of three dynamic frames of the knee with the CoCr femoral implant and three dynamic frames of the knee with the Zr femoral implant were rated. As the material of the tibial component was the same for both cadavers, the questions related to the tibia were left out of consideration. The dynamic frames were obtained with the same kV, mAs and reconstruction technique (i.e. 120 kV, 7 mAs, non-SEMAR and a bone kernel) for both implants. All reconstructions were displayed in a bone window.

Table 3: Subjective evaluation criteria for qualitative image analysis.

Q1: Visibility of the patella				
Very poor (1)	Poor (2)	Moderate (3)	Good (4)	Very good (5)
Q2: Visibility of the femoral condyles				
Very poor (1)	Poor (2)	Moderate (3)	Good (4)	Very good (5)
Q3: Visibility of the proximal tibia				
Very poor (1)	Poor (2)	Moderate (3)	Good (4)	Very good (5)
Q4: Visibility of the femoral component				
Very poor (1)	Poor (2)	Moderate (3)	Good (4)	Very good (5)
Q5: Visibility of the tibial component				
Very poor (1)	Poor (2)	Moderate (3)	Good (4)	Very good (5)
Q6: Presence of metal and motion artifacts				
Maximum (1)	Heavy (2)	Moderate (3)	Minimum (4)	Absent (5)

2.2.2. Quantitative image analysis

The influence of tube voltage, tube current and reconstruction technique on static CT image quality was quantitatively assessed. The mean attenuation value, image noise and Signal-to-Noise Ratio (SNR) of the patellae from the post TKA static CT reconstructions of the knee with the CoCr implant were calculated using MATLAB (version 2020a, MathWorks, Natick, Massachusetts, United States). The patella was segmented using 3D Slicer (version 4.10.2) [16]. Segmentation was performed by thresholding on HU followed by manual fine-tuning (i.e. painting, erasing and smoothing). The post TKA static CT reconstructions were masked with the segmented patella and from the voxels within the masked volume, the mean attenuation value in HU was calculated. Image noise was defined as the standard deviation (SD) in HU within the masked volume. SNR was calculated by dividing the mean attenuation value by the image noise.

2.2.3. Effective dose calculation

The influence of tube voltage and tube current on the radiation dose was investigated by calculating the effective dose (ED) of each static CT scan and each dynamic CT data set by multiplication of the measured dose length product (DLP) with a DLP/ED conversion coefficient of 0.0004 mSv/(mGy·cm) [18].

2.3. Assessing the patellar tracking pattern

To assess the patellar tracking pattern before versus after TKA from dynamic CT data, the positions of the bones and implant components were determined first through segmentation and registration. Subsequently, based on these positions of the bones and implant components, patellar motion analysis was performed, in which the patellar tracking pattern was assessed in terms of patellar flexion, tilt, rotation and shift. In Appendix 1, it is described which steps were taken to design this method, it is discussed which methods were not sufficient and recommendations for future optimisation of the method are provided.

2.3.1. Segmentation

From the pre TKA static CT scan and from four different pre TKA dynamic CT frames (i.e. the frame with the maximum tibiofemoral flexion angle, the frame with the minimum tibiofemoral flexion angle and two frames in between), the femur, tibia and patella were segmented using a 3D Dense-U-Net neural network [19]. From the post TKA static CT reconstruction with the least artifacts and the best visibility of the bones and implant components, the femur, femoral component, tibia, tibial component and patella were segmented using 3D Slicer (version 4.10.2) [16]. Segmentation was performed by thresholding on HU followed by manual fine-tuning (i.e. painting, erasing and smoothing). Similarly, from four different dynamic CT frames of the post TKA dynamic CT reconstruction set with the least artifacts and the best visibility of the bones and implant components, the femoral component, tibial component and patella were segmented.

2.3.2. Registration

Rigid point cloud registration was used to register the femur, tibia and patella from the pre TKA static CT scan to respectively the femur, tibia and patella from each of the four pre TKA dynamic CT frames. This resulted in a transformation (rotation and translation) referred to as $T_{pre\ static \rightarrow pre\ dynamic}$ for the femur, patella and tibia for each of the four dynamic frames. Rigid point cloud registration was performed using the Coherent Point Drift (CPD) algorithm [20] in MATLAB. The post TKA static femoral component, tibial component and patella were registered to respectively the femoral component, tibial component and patella from of each of the four post TKA dynamic CT frames using rigid binary mask registration followed by rigid image registration in Elastix (version 5.0.1) [21,22]. This provided the transformation $T_{post\ static \rightarrow post\ dynamic}$ of the femoral component, tibial component and patella for each of the four dynamic frames. The pre TKA static bones were registered with the post TKA static bones using rigid point cloud registration (CPD algorithm) in MATLAB, giving the transformation $T_{pre\ static \rightarrow post\ static}$ for the femur, tibia and patella. Finally, the manufacturers Computer-Aided Design (CAD) model of the femoral component was registered to the femoral component from the post TKA static scan using rigid point cloud registration (CPD algorithm) in MATLAB, providing the transformation $T_{CAD \rightarrow post\ static}$ of the femoral component. A schematic overview of the segmentation and registration process is shown in Figure 2.

2.3.3. Patellar motion analysis

The patellar tracking pattern was assessed by determining the patellar flexion, tilt, rotation and shift at the four different tibiofemoral flexion angles. Motion analysis was based on the anatomical coordinate system of the human knee as proposed by Miranda et al. [23]. Based on this coordinate system, the femoral, patellar and tibial anatomical reference frames of the pre TKA static bones were calculated. The anatomical reference frames consisted of an anteroposterior (AP), mediolateral (ML) and proximodistal (PD) axis. An example of a segmented femur, patella and tibia with their anatomical reference frames is shown in Figure 3. The previously found transformations were applied to the anatomical reference frames of the pre TKA static bones to obtain the anatomical reference frames of the pre TKA dynamic, post TKA static and post TKA dynamic bones. As the femur and femoral component were fixated, the transformation $T_{post\ static \rightarrow post\ dynamic}$ of the femoral component could be applied to the static post TKA femoral anatomical reference frame to obtain the dynamic post TKA femoral anatomical reference frame. Accordingly, the transformation $T_{post\ static \rightarrow post\ dynamic}$ of the tibial component could be applied to the static post TKA tibial anatomical reference frame to obtain the dynamic post TKA tibial anatomical reference frame.

For the pre TKA and post TKA dynamic frames, Euler angles were calculated for the patellar anatomical reference frame with respect to the femoral anatomical reference frame. Patellar flexion was described by the first Euler angle, patellar tilt was described by the second Euler angle and patellar rotation was described by the third Euler angle. Patellar flexion was defined as the rotation of the patella about the femoral ML axis. Patellar flexion was positive when the distal apex of the patella moved posteriorly relative to the proximal pole. Patellar tilt was defined as the rotation of the patella about the femoral PD axis. Patellar tilt was positive when the lateral edge of the patella rotated towards the femur relative to the medial edge of the patella (lateral tilt). Patellar rotation was defined as the rotation of the patella about the femoral AP axis. Patellar rotation was positive when the distal pole of the patella moved medially relative to the proximal pole of the patella (medial rotation). Patellar shift was defined as the translation of the patella along the femoral ML axis. Patellar shift was positive when the patella shifted medially along the femoral ML axis (medial shift). [24]

Patellar tracking was visualized by projecting the origin of the patellar anatomical reference frame on the (native or implant) femoral trochlea along the patellar AP axis for each of the four tibiofemoral flexion angles. The tibiofemoral flexion angles were determined by calculation of the Euler angles of the tibial anatomical reference frames with respect to the femoral anatomical reference frame. The tibiofemoral flexion angle was then described by the first Euler angle, which was defined as the rotation of the tibia about the femoral ML axis.

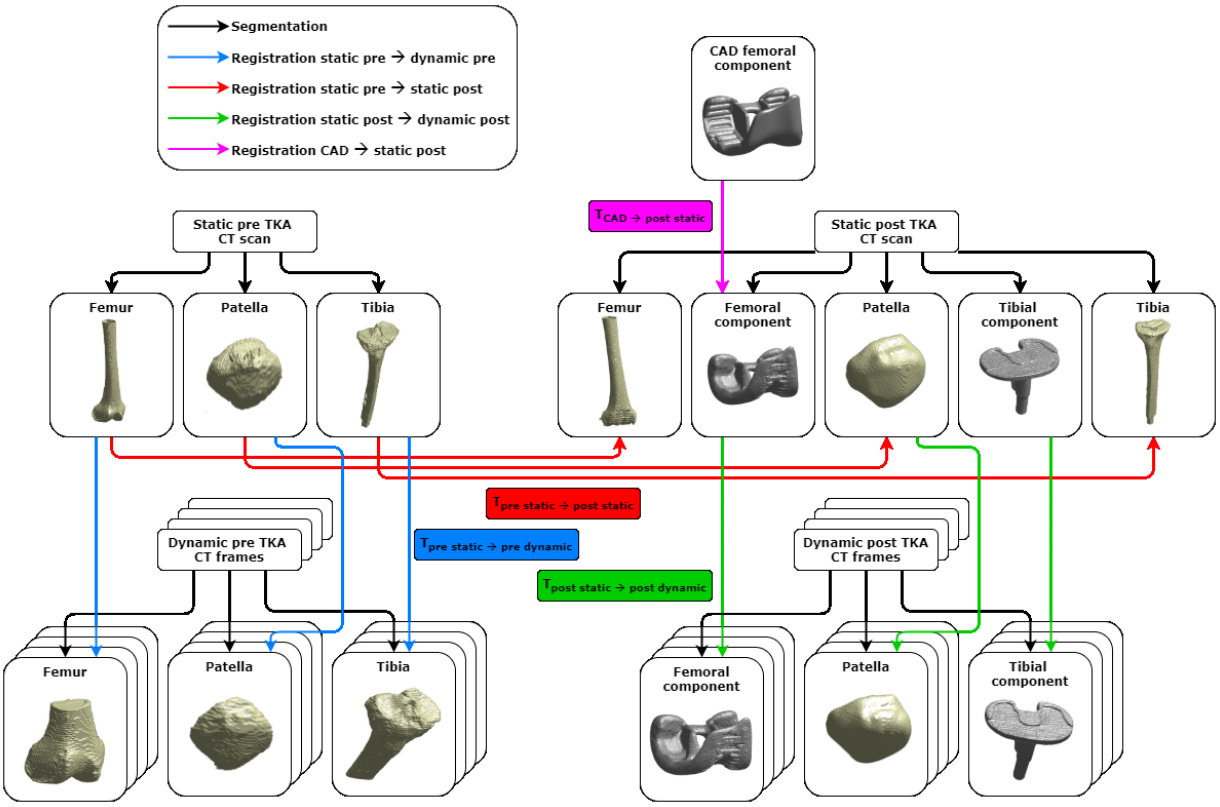

Figure 2: Schematic overview of the segmentation and registration process.

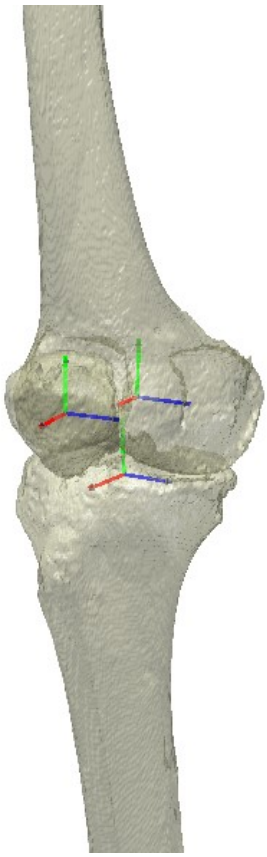

Figure 3: Example of segmented femur, tibia and patella with their anatomical reference frames. The anteroposterior axis is indicated with a red arrow (with the arrow pointing anteriorly), the mediolateral axis is indicated with a blue arrow (with the arrow pointing medially) and the proximodistal axis is indicated with a green arrow (with the arrow pointing proximally).

3. Results

The results of the search for a suitable dynamic CT imaging method is provided first. This is followed by the results of the assessment of the patellar tracking pattern before versus after TKA.

3.1. Search for suitable dynamic CT imaging method

A complete overview of the results is shown in Appendix 2, where the results of the qualitative image analysis on the influence of CT imaging parameters on image quality are presented in Table A for the static CT images and in Table B for the dynamic CT data sets. In Table C, the results of the qualitative image analysis on the influence of the implant material on image quality are presented. Table D presents the results of the quantitative image analysis on the influence of CT imaging parameters on image quality. The effective doses of the static and dynamic CT scans are shown in Table 4.

3.1.1. Qualitative image analysis

For the static non-SEMAR reconstructions, increasing the tube voltage and tube current improved the visibility of the patella and the femoral component and lowered the presence of metal artifacts. For the static SEMAR reconstructions, increasing the tube voltage and tube current did not change the visibility of the patella at all. The visibility of the femoral component scored best at the lowest tube voltage and tube current for the static SEMAR soft tissue reconstructions. For the static SEMAR bone reconstructions, there was no clear relationship between the tube voltage and tube current and the visibility of the femoral component. In addition, there was no clear relationship between tube voltage and tube current and the presence of metal artifacts for all static SEMAR reconstructions. For the static non-SEMAR reconstructions, the soft tissue and bone kernel received the same score at the lowest kV and mAs. At the highest kV and mAs, the bone kernel received the best score. At intermediate kV and mAs, the static soft tissue reconstructions scored better than the static bone reconstructions. For the static SEMAR reconstructions, there was no clear relationship between reconstruction kernel and visibility of the bones and implant components or presence of metal artifacts. Furthermore, the use of the SEMAR algorithm did not seem to improve the visibility of the bones and implant components and the presence of metal artifacts in the static CT reconstructions. Examples of static CT images reconstructed with either a soft tissue or a bone kernel and either with or without the SEMAR algorithm are shown in Figure 4. From this figure it can be noticed that the static CT images reconstructed with a soft tissue kernel have a lower spatial resolution than the static CT images reconstructed with a bone kernel. Moreover, in the static CT images reconstructed with the SEMAR algorithm, new streak artifacts can be observed and the posterior edge of the patella has disappeared.

For the dynamic non-SEMAR soft tissue reconstruction sets, increasing the tube voltage and tube current improved the visibility of the patella and the femoral component. The presence of metal and motion artifacts did not change. For the dynamic non-SEMAR bone reconstruction sets, there was no clear relationship between tube voltage and tube current and visibility of the of the patella. The visibility of the femoral component did not change. The presence of metal and motion artifacts improved with an increasing tube voltage and

tube current. For the dynamic SEMAR reconstruction sets, the visibility of the patella improved with an increasing tube voltage and tube current. The presence of metal and motion artifacts did not change with an increasing tube voltage and tube current. For the dynamic SEMAR soft tissue reconstruction sets, there was no clear relationship between tube voltage and tube current and visibility of the femoral component. For the dynamic SEMAR bone reconstruction sets, increasing the tube voltage and tube current did not affect the visibility of the femoral component. For the dynamic non-SEMAR reconstruction sets, there was no clear relationship between reconstruction kernel and visibility of the patella. The use of a soft tissue reconstruction kernel improved the visibility of the femoral component and lowered the presence of metal and motion artifacts. For the dynamic SEMAR reconstruction sets, there was no clear relationship between reconstruction kernel and visibility of the bones and implant components. The presence of metal and motion artifacts remained the same. Furthermore, the use of the SEMAR algorithm did not seem to improve the visibility of the bones and implant components and the presence of metal artifacts in the dynamic CT reconstruction sets. Examples of dynamic CT images reconstructed with either a soft tissue or a bone kernel and either with or without the SEMAR algorithm are shown in Figure 5. From this figure it can be noticed that the dynamic CT images reconstructed with a soft tissue kernel have a lower spatial resolution than the dynamic CT images reconstructed with a bone kernel. Moreover, in the dynamic CT images reconstructed with the SEMAR algorithm, new streak artifacts can be observed and the posterior edge of the patella has disappeared.
The dynamic CT reconstruction sets scored lower than the static CT reconstructions on the visibility of the bones and implant components and on the presence of metal and motion artifacts. Furthermore, the CoCr implant resulted in an overall better visibility of the bones and implant components and less metal and motion artifacts than the Zr implant.

3.1.2. Quantitative image analysis

The mean HU decreased with an increasing tube voltage and tube current for all reconstructions, except for the non-SEMAR bone reconstructions, where the 120 kV 40 mAs reconstruction had a higher mean HU than the reconstructions obtained at the other kV and mAs settings. Image noise decreased as well with an increasing tube voltage and tube current for all reconstructions, except for the reconstructions obtained at the highest kV and mAs settings, where the image noise increased. For the non-SEMAR soft tissue reconstructions, SNR decreased with an increasing tube voltage and tube current. For the non-SEMAR bone and for the SEMAR reconstructions, there was no clear relationship between tube voltage and tube current and SNR. Images reconstructed with a soft tissue kernel had less noise and a better SNR than images reconstructed with a bone kernel. SEMAR reconstructions had a higher SNR than non-SEMAR reconstructions but also a higher image noise.

3.1.3. Effective dose calculation

The ED of the static and dynamic CT data obtained at different tube voltages and exposures is shown in Table 4. Increasing the tube voltage and tube current increased the effective dose. Dynamic scanning resulted in a higher effective dose than static scanning.

Table 4: Effective dose (mSv) of the static and dynamic CT data obtained at different tube voltages (kV) and exposures (mAs).

	Tube voltage (kV)	Exposure (mAs)	Effective dose (mSv)
Static	100	10	0.008
	120	10	0.014
	120	40	0.055
	120	150	0.207
Dynamic	100	7	0.069
	120	7	0.125
	120	17	0.313

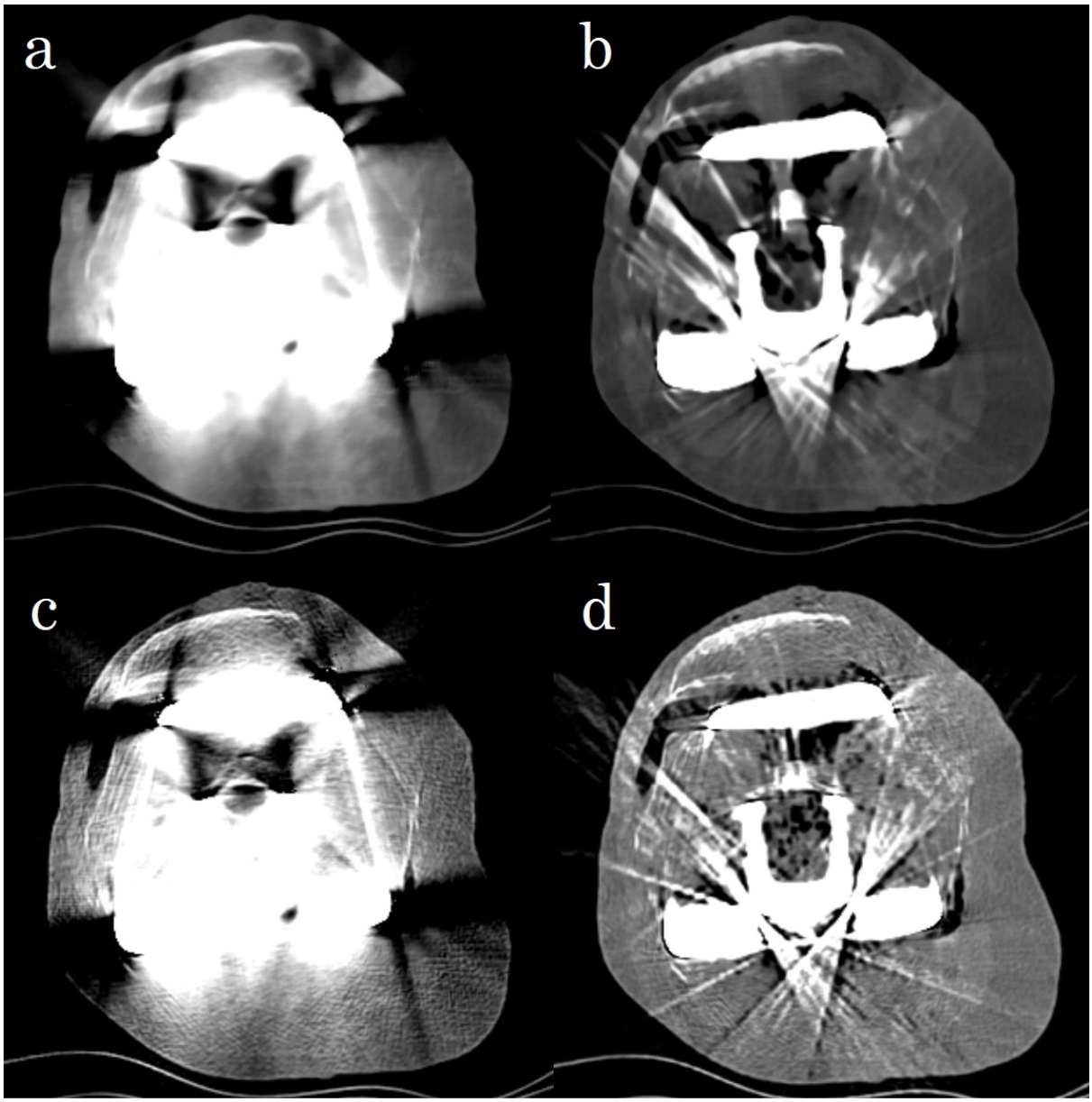

Figure 4: Axial CT slices of static a) non-SEMAR soft tissue, b) SEMAR soft tissue, c) non-SEMAR bone and d) SEMAR bone reconstructions obtained at 120 kV and 40 mAs. All reconstructions are displayed in a bone window (window width of 1800 HU and window level of 400 HU).

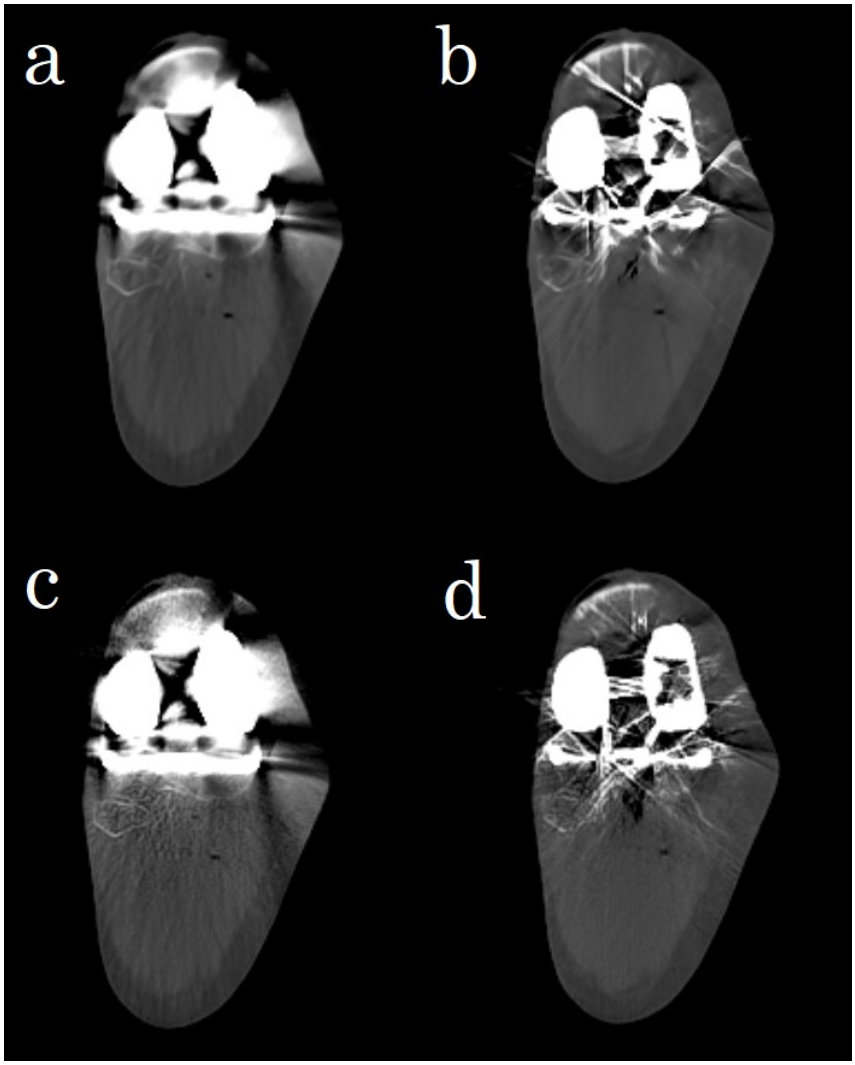

Figure 5: Axial CT slices of dynamic a) non-SEMAR soft tissue, b) SEMAR soft tissue, c) non-SEMAR bone and d) SEMAR bone reconstructions obtained at 120 kV and 17 mAs. All reconstructions are displayed in a bone window (window width of 1800 HU and window level of 400 HU).

3.2. Assessing the patellar tracking pattern

The maximum tibiofemoral flexion angle in the pre TKA dynamic CT data set was 55°. The minimum tibiofemoral flexion angle was 12° and the frames in between had a tibiofemoral flexion angle of 25° and 36°. In the post TKA dynamic CT data set, the maximum tibiofemoral flexion angle was 62°, the minimum tibiofemoral flexion angle was 8° and the frames in between had a tibiofemoral flexion angle of 16° and 42°.

The pre and post TKA patellar flexion, tilt, rotation and shift at the four different tibiofemoral flexion angles are shown in Figure 6. Differences could be observed between the pre and post TKA patellar flexion, tilt, rotation and shift. These differences are described in Appendix 3.

To visualize the patellar tracking pattern pre and post TKA, a projection of the origin of the patellar anatomical reference frame along the patellar AP axis on the (native or implant) femoral trochlea is depicted in Figure 7 for each of the four tibiofemoral flexion angles. Differences between the pre and post TKA patellar tracking pattern could be observed. These differences are described in Appendix 3.

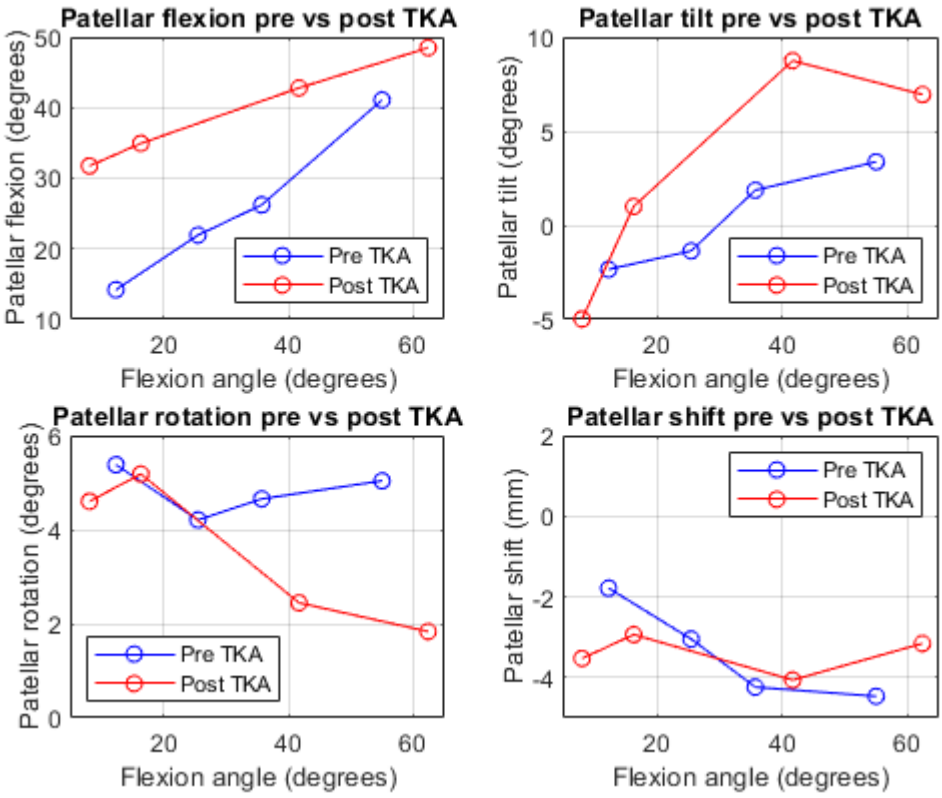

Figure 6: Pre (blue) and post (red) TKA patellar flexion (top left), patellar tilt (top right), patellar rotation (bottom left) and patellar shift (bottom right). Positive patellar flexion indicates that the distal apex of the patella moves posteriorly relative to the proximal pole, positive patellar tilt indicates lateral tilt, positive patellar rotation indicates medial rotation and positive patellar shift indicates medial shift.

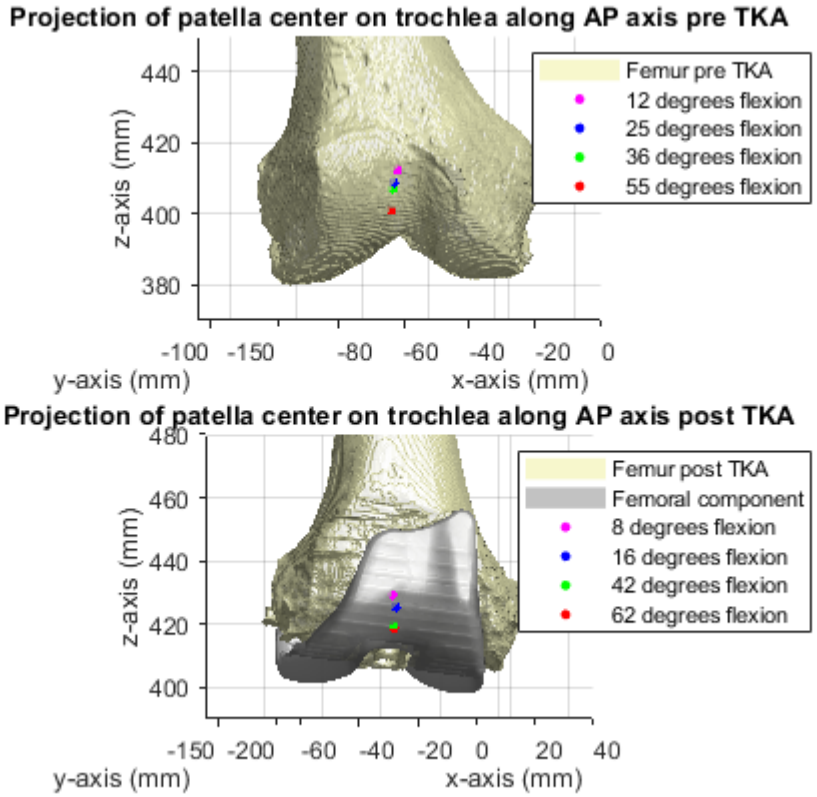

Figure 7: Visualisation of pre (upper) and post (lower) TKA patellar tracking pattern by projection of the origin of the patellar anatomical reference frame on the (native or implant) femoral trochlea along the patellar AP axis for each of the four tibiofemoral flexion angles. Left in the image is lateral and right is medial.

4. Discussion

In this study, it was investigated to what extent dynamic CT can be used to assess the patellar tracking pattern before versus after TKA. The first part of this study aimed at finding a suitable method to image a knee after TKA with dynamic CT. The second part of this study aimed at developing a technique to assess the patellar tracking pattern before versus after TKA from dynamic CT data.

The static CT reconstruction that provided the best overall image quality according to the qualitative image analysis was the reconstruction obtained at the highest kV and mAs, without the SEMAR algorithm and with a bone reconstruction kernel. Therefore, this static CT reconstruction was used for assessing the patellar tracking pattern. The dynamic CT reconstruction set that provided the best image quality according to the qualitative image analysis was the reconstruction set obtained at the highest kV and mAs without the SEMAR algorithm and with a soft tissue reconstruction kernel. However, usage of a soft tissue reconstruction kernel is known to reduce the spatial resolution. Therefore, the dynamic CT reconstruction set obtained at the highest kV and mAs without the SEMAR algorithm and with a bone reconstruction kernel was used for assessing the patellar tracking pattern instead.
Considering the effective dose and thereby making a trade-off between image quality and radiation dose, it is recommended to obtain static CT data of patients post TKA at 120 kV and 10 mAs and dynamic CT data at 120 kV and 7 mAs. This results in a total effective dose of 0.139 mSv (0.014 mSv for the static scan and 0.125 mSv for the dynamic scan). The effective dose of the pre TKA static and dynamic scan is 0.077 mSv (0.008 mSv for the static scan and 0.069 mSv for the dynamic scan). For both the static and the dynamic CT data, non-SEMAR reconstructions with a bone reconstruction kernel are recommended. Furthermore, it is recommended to implant a CoCr instead of a Zr femoral component as this results in less metal artifacts. This is most likely due to the lower atomic number of CoCr compared with Zr .
Increasing the CT tube voltage and tube current is known to reduce artifacts and improve image quality [14,25,26]. This is in line with the majority of the findings in our study. However, in our quantitative image analysis, increasing the exposure from 40 mAs to 150 mAs resulted in an inexplicable increase in image noise and a decrease in SNR. Previous literature also found that implantation of a CoCr instead of a Zr implant reduces metal artifacts [14,26]. This is in accordance with the findings of our study. Usage of a soft tissue reconstruction kernel instead of a bone reconstruction kernel is also known to reduce the visibility of artifacts and decrease image noise [14]. This is in line with the results of the quantitative image analysis, as the images reconstructed with a soft tissue kernel had a lower image noise and a higher SNR than the images reconstructed with a bone kernel. In the qualitative image analysis of our study, it was dependent on the tube voltage and tube current and on the static or dynamic imaging whether the reconstructions obtained with a soft tissue or a bone kernel received a higher score. A disadvantage of using a soft tissue reconstruction kernel is that it reduces the spatial resolution of the image [14]. In our study, it was also noticed that the soft tissue reconstructions had a lower spatial resolution than the bone reconstructions. Due to the smoothing, the edges of the patella

were less sharp in the soft tissue reconstructions. This was not desirable, as it was expected to reduce the accuracy of the segmentation and registration process.
The results of our study also suggest that the use of a SEMAR algorithm does not improve the visibility of the bones and implant components and the presence of metal artifacts. To understand this, it should first be understood how the SEMAR algorithm works. The SEMAR algorithm first generates an original image from the original sinogram by Filtered Back-Projection (FBP). Metal is segmented from this original image to generate a metal-only image, which is then forward projected to obtain a metal-only sinogram. Subsequently, a metal-free sinogram is created by estimation of the metal corrupted sinogram data. A prior image is then generated from the metal-free sinogram by FBP, to which a gradient optimization process is applied via forward projection. This gradient optimization process smoothes transitions in the sinogram while maintaining image edge content. FBP is then used again to obtain the final metal-free image. The final SEMAR image is created by adding the previously segmented metal to the metal-free image. The effectiveness of the SEMAR algorithm depends highly on the estimation of the metal corrupted sinogram data. Sharp transitions between the original sinogram data and the estimated sinogram data can result in new streak artifacts. [15] Although the gradient optimization process should prevent this by smoothing sharp transitions, we could still observe some new streak artifacts in our SEMAR images (Figure 4 and Figure 5). This is in accordance with previous literature, where the SEMAR algorithm was also found to reduce the original artifacts while introducing new artifacts [14,27–29]. Furthermore, although the gradient optimization process is claimed to preserve edges, the posterior edge of the patella was completely lost in the SEMAR images (Figure 4 and Figure 5). This was undesirable for this study, as it hampered the segmentation of the patella. In addition, the estimated HU values in the SEMAR images seemed incorrect, especially in areas close to metal edges. This would also hamper the (HU-based) segmentation and registration process. Thus, although the SEMAR images appeared less blurry than the non-SEMAR images and the large black and white streaks were lost, new streak artifacts appeared, crucial edges were lost and estimated HU values seemed incorrect. Therefore, we do not recommend the use of images reconstructed with the SEMAR algorithm for the assessment of the patellar tracking pattern.

A technique for the assessment of the patellar tracking pattern before versus after TKA using dynamic CT was developed. Differences were found between the pre and post TKA patellar flexion, tilt, rotation and shift. To our knowledge, this was the first study that used dynamic CT after TKA to assess the patellar tracking pattern. However, other researchers aimed to assess the patellar tracking pattern after TKA as well. Single-plane fluoroscopy, biplanar radiography, static CT and static MRI have all been investigated.
Sharma et al. [30] used dynamic single-plane sagittal fluoroscopy in combination with static CT to measure the patellar tracking pattern post TKA. An advantage of their method is the possibility to assess the patellar tracking pattern dynamically under weight-bearing circumstances. A limitation of their method is that it relies on projected 2D images, and therefore requires 3D-to-2D registration. The accuracy of the motions in the mediolateral direction, which are in fact the motions that are of most interest, is therefore expected to be poorer than with the method that was described in our study, as

our method relies on 3D-to-3D registration. Another limitation of their method is that it is dependent on the placement of a patellar component.

Shandiz et al. [31] and Sharma et al. [32] used sequential biplanar sagittal radiography at eight different knee flexion angles in combination with static CT to investigate pre and post TKA patellofemoral weightbearing kinematics. An advantage of biplanar radiography compared to single-plane radiography is the improved reliability for motions in the mediolateral direction. However, it still requires 3D-to-2D registration, and thus the accuracy of the motions in the mediolateral direction is expected to be less accurate than with the method that was described in our study. Another limitation of biplanar radiography is that the observed movement is not truly dynamic, as it is based sequential static images at different flexion angles. Moreover, their methods also depend on the placement of a patellar component. Sharma et al. [32] compared the poses of the bones and implant components from the sequential biplane images with the poses from the CT scans. They found an absolute difference of 0.88° for patellar flexion, 0.58° for patellar tilt, 0.41° for patellar rotation and 0.13 mm for patellar shift. The mean interobserver repeatability of their method was 2.01° for patellar flexion, 2.77° for patellar tilt, 1.87° for patellar rotation and 1.20 mm for patellar shift. The mean intraobserver repeatability of their method was 1.98° for patellar flexion, 1.67° for patellar tilt, 1.28° for patellar rotation and 1.85 mm for patellar shift.

Ho et al. [33] imaged subjects before and after TKA with CT at 0° and 30° knee flexion while they pushed against a weight, providing static muscular activation. With this method, they were able to measure patellar flexion, tilt and shift. A limitation of their method compared to the method that was developed in our study is that the observed movement was not truly dynamic, as it was based on static CT images at different flexion angles. Furthermore, flexion angles greater than 30° could not be reached. In addition, the method was dependent on the placement of a patellar component. Ho et al. [33] compared the poses of the bones and implant components from the CT images with the poses from a coordinate measuring machine and found an absolute difference of 0.24° for patellar flexion, 0.19° for patellar tilt and 0.18 mm for patellar shift. The repeatability of their 3D-to-3D registration method was 0.29° or less for rotation and 0.11 mm or less for translation.

Von Eisenhart-Rothe et al. [34] measured the patellar shift and tilt of healthy volunteers and post TKA patients in an open Magnetic Resonance Imaging (MRI) scanner at 0°, 30° and 90° knee flexion under static muscular activation. A limitation of their method compared to the method that was developed in our study is that the observed movement was not truly dynamic, as it was based on static magnetic resonance images at different flexion angles. Furthermore, the method was dependent on the placement of a patellar component. Moreover, compared with CT, usage of MRI to image subjects post TKA creates metal artifacts as well and the implant metal may distort the magnetic field. In addition, MRI has a lower spatial resolution and is more expensive, less available and more time-consuming than CT. [33]

To date, none of the previously described methods have made their translation to daily clinical practice. Furthermore, the difference in methodology between studies investigating pre and post TKA patellofemoral kinematics hampers a fair comparison. Therefore, it is necessary to reach consensus on a method for assessing patellar tracking before and after TKA. We propose dynamic CT, as it is a relatively fast, simple,

inexpensive and accessible technique. Furthermore, the observed movement is truly dynamic and the method relies on 3D-to-3D registration, which is expected to be more accurate than the 3D-to-2D registration that is used in fluoroscopy and biplanar radiography, especially for movements in the mediolateral direction. Additionally, the previously described studies used different coordinate systems to describe patellar kinematics pre and post TKA. Pre TKA, anatomical coordinate systems were computed. Post TKA, prosthesis coordinate systems, using design features of the prosthesis components, were computed. Our method uses anatomical coordinate systems both pre and post TKA, which is expected to make the comparison between pre and post TKA kinematics more accurate. Moreover, our method does not rely on the placement of a patellar component. This is an advantage, as the placement of a patellar component is controversial [35].

A limitation of this study is the absence of quadriceps muscle activation due to the passive motion of the cadaveric knee. Furthermore, a right knee was implanted with a left femoral component as a right femoral component was not available. Consequently, the observed patellar tracking pattern is not representative for the actual patellar tracking pattern in a patient. However, when applying the proposed method to patients instead of cadaveric knees, the patellar tracking pattern can actually be studied under muscular activation and with the correct femoral component implanted. Another limitation of this study is that only 4 of the 41 dynamic frames were analysed because of the time-consuming segmentation and registration process. Therefore, we recommend to automate this process in the near future. This would enable all patellofemoral flexion angles to be studied. Automatization could for example be achieved by training a convolutional neural network with CT scans affected by metal artifacts [36]. It might also be investigated whether segmentation of the patella can be automated, for example by edge detection of the anterior surface of the patella, as the anterior surface is least affected by metal artifacts. Another limitation is that the method that was proposed in this study to assess the patellar tracking pattern cannot create weight-bearing circumstances. Weight-bearing circumstances can be achieved with fluoroscopy. Nevertheless, fluoroscopic analysis is expected to be less accurate for motions in the mediolateral direction, which are in fact the movements that are of most interest. Finally, although it has been attempted to move the cadaveric knees at a constant velocity, an exact same velocity for each of the dynamic CT frames in one data set and between the dynamic data sets with a different kV, mAs and femoral implant could not be assured. As motion artifacts are expected to be higher for objects with a higher velocity, this might have hampered a fair comparison. Additionally, increased motion artifacts are expected to complicate the segmentation and registration process. It would therefore be advised to aim at maintaining a constant velocity during the flexion and extension movement of the knee when imaging patients with dynamic CT.

Future research should investigate the accuracy and precision of the proposed method. It can however be reasoned that the accuracy and precision depend on several factors, the most import of which is the spatial resolution of the CT images. The spatial resolution of the CT images influences the accuracy and precision of the segmentation process and image registration process. The spatial resolution is for example affected by slice thickness, pixel spacing, reconstruction kernel and motion. The maximum slice thickness

and pixel spacing of the CT images that were used in this study was 1 mm. A bone reconstruction kernel was used, as this provided a better spatial resolution than a soft tissue reconstruction kernel. The accuracy of the point cloud registrations relied on the accuracy of the segmentations, but also on the accuracy of the registration algorithm. The CPD rigid point cloud registration algorithm that was used in this study has an accuracy of less than 0.1° in determining the rotation matrix, even with a lot of noise and outliers in the point sets [20]. Moreover, the precision is influenced by the inter- and intraobserver variability of the segmentations, but these were not examined in this study.

For future research, it is also strongly recommended to automate the segmentation and registration process. This can speed up the process, thereby enabling more flexion angles to be studied in a shorter period of time. Moreover, it would offer the possibility to apply the method to a larger patient population. These patients may then be asked to complete a questionnaire on anterior knee pain, for example the Kujala questionnaire [37,38]. Subsequently, the relationship between (a change in) the patellar tracking pattern after TKA and anterior knee pain could be clarified. Insight in how the patellar tracking pattern might contribute to anterior knee pain may potentially guide orthopaedic surgeons in their surgical approach, ultimately improving TKA outcomes and preventing revision surgeries.

5. Conclusion

A method for the assessment of the patellar tracking pattern before versus after TKA using dynamic CT was successfully developed. Future research to the accuracy and precision of the developed method should be performed. Furthermore, automation of the segmentation and registration process is advised. Subsequently, the developed method can be used to clarify the relationship between (a change in) the patellar tracking pattern after TKA and anterior knee pain. This may potentially guide orthopaedic surgeons in their surgical approach, ultimately improving TKA outcomes and preventing revision surgeries.

References

[1] Cross M, Smith E, Hoy D, Nolte S, Ackerman I, Fransen M, et al. The global burden of hip and knee osteoarthritis: Estimates from the Global Burden of Disease 2010 study. Ann Rheum Dis 2014;73:1323–30. https://doi.org/10.1136/annrheumdis-2013-204763.

[2] Carr AJ, Robertsson O, Graves S, Price AJ, Arden NK, Judge A, et al. Knee replacement. Lancet, vol. 379, Lancet Publishing Group; 2012, p. 1331–40. https://doi.org/10.1016/S0140-6736(11)60752-6.

[3] Michalik R, Rath B, Springorum HR, Lüring C, Tingart M. Vorderer Knieschmerz nach Knie-TEP-Implantation: Ursachen, Diagnostik und Therapie. Orthopade 2016;45:386–98. https://doi.org/10.1007/s00132-016-3256-7.

[4] Dutch Arthroplasty Register (LROI). Online LROI annual report 2020. https://www.lroi-report.nl/app/uploads/2021/03/PDF-LROI-annual-report-2020.pdf (accessed June 10, 2021).

[5] Shervin D, Pratt K, Healey T, Nguyen S, Mihalko WM, El-Othmani MM, et al. Anterior knee pain following primary total knee arthroplasty. World J Orthop 2015;6:795–803. https://doi.org/10.5312/wjo.v6.i10.795.

[6] Petersen W, Rembitzki IV, Brüggemann GP, Ellermann A, Best R, Koppenburg AG, et al. Anterior knee pain after total knee arthroplasty: A narrative review. Int Orthop 2014;38:319–28. https://doi.org/10.1007/s00264-013-2081-4.

[7] Laubach M, Hellmann JTR, Dirrichs T, Gatz M, Quack V, Tingart M, et al. Anterior knee pain after total knee arthroplasty: A multifactorial analysis. J Orthop Surg 2020;28:1–12. https://doi.org/10.1177/2309499020918947.

[8] Post WR, Teitge R, Amis A. Patellofemoral malalignment: Looking beyond the viewbox. Clin Sports Med 2002;21:521–46. https://doi.org/10.1016/S0278-5919(02)00011-X.

[9] Barink M, Meijerink H, Verdonschot N, Van Kampen A, De Waal Malefijt M. Asymmetrical total knee arthroplasty does not improve patella tracking: A study without patella resurfacing. Knee Surgery, Sport Traumatol Arthrosc 2007;15:184–91. https://doi.org/10.1007/s00167-006-0158-y.

[10] Barink M, Van de Groes S, Verdonschot N, De Waal Malefijt M. The difference in trochlear orientation between the natural knee and current prosthetic knee designs; towards a truly physiological prosthetic groove orientation. J Biomech 2006;39:1708–15. https://doi.org/10.1016/j.jbiomech.2005.04.027.

[11] Cho WS, Woo JH, Park HY, Youm YS, Kim BK. Should the “no thumb technique” be the golden standard for evaluating patellar tracking in total knee arthroplasty? Knee 2011;18:177–9. https://doi.org/10.1016/j.knee.2010.04.009.

[12] Jibri Z, Jamieson P, Rakhra KS, Sampaio ML, Dervin G. Patellar maltracking: an update on the diagnosis and treatment strategies. Insights Imaging 2019;10:65. https://doi.org/10.1186/s13244-019-0755-1.

[13] Boas FE, Fleischmann D. CT artifacts: Causes and reduction techniques. Imaging Med 2012;4:229–40. https://doi.org/10.2217/iim.12.13.

[14] Wellenberg RHH, Hakvoort ET, Slump CH, Boomsma MF, Maas M, Streekstra GJ. Metal artifact reduction techniques in musculoskeletal CT-imaging. Eur J Radiol 2018;107:60–9. https://doi.org/10.1016/j.ejrad.2018.08.010.

[15] Zhang D, Angel E. Single Energy Metal Artifact Reduction: A Reliable Metal Management Tool in CT. 2017.

[16] Fedorov A, Beichel R, Kalpathy-Cramer J, Finet J, Fillion-Robin JC, Pujol S, et al. 3D Slicer as an image computing platform for the Quantitative Imaging Network. Magn Reson Imaging 2012;30:1323–41. https://doi.org/10.1016/j.mri.2012.05.001.

[17] Seroul P, Sarrut D. VV: A viewer for the evaluation of 4D image registration. Midas J 2008:1–8.
[18] Saltybaeva N, Jafari ME, Hupfer M, Kalender WA. Estimates of effective dose for CT scans of the lower extremities. Radiology 2014;273:153–9. https://doi.org/10.1148/radiol.14132903.
[19] Kolařík M, Burget R, Uher V, Říha K, Dutta MK. Optimized high resolution 3D dense-U-Net network for brain and spine segmentation. Appl Sci 2019;9:404. https://doi.org/10.3390/app9030404.
[20] Myronenko A, Song X. Point set registration: Coherent point drifts. IEEE Trans Pattern Anal Mach Intell 2010;32:2262–75. https://doi.org/10.1109/TPAMI.2010.46.
[21] Klein S, Staring M, Murphy K, Viergever MA, Pluim JPW. elastix: A Toolbox for Intensity-Based Medical Image Registration. IEEE Trans Med Imaging 2010;29. https://doi.org/10.1109/TMI.2009.2035616.
[22] Shamonin DP, Bron EE, Lelieveldt BPF, Smits M, Klein S, Staring M. Fast parallel image registration on CPU and GPU for diagnostic classification of Alzheimer's disease. Front Neuroinform 2014;7. https://doi.org/10.3389/fninf.2013.00050.
[23] Miranda DL, Rainbow MJ, Leventhal EL, Crisco JJ, Fleming BC. Automatic determination of anatomical coordinate systems for three-dimensional bone models of the isolated human knee. J Biomech 2010;43:1623–6. https://doi.org/10.1016/j.jbiomech.2010.01.036.
[24] Bull AMJ, Katchburian M V., Shih YF, Amis AA. Standardisation of the description of patellofemoral motion and comparison between different techniques. Knee Surgery, Sport Traumatol Arthrosc 2002;10:184–93. https://doi.org/10.1007/s00167-001-0276-5.
[25] Frey GD. Basic CT Parameters. AJR 2014;203:W126–7. https://doi.org/10.2214/AJR.13.10994.
[26] De Crop A, Casselman J, Van Hoof T, Dierens M, Vereecke E, Bossu N, et al. Analysis of metal artifact reduction tools for dental hardware in CT scans of the oral cavity: kVp, iterative reconstruction, dual-energy CT, metal artifact reduction software: does it make a difference? Neuroradiology 2015;57:841–9. https://doi.org/10.1007/s00234-015-1537-1.
[27] Barreto I, Pepin E, Davis I, Dean C, Massini T, Rees J, et al. Comparison of metal artifact reduction using single-energy CT and dual-energy CT with various metallic implants in cadavers. Eur J Radiol 2020;133:1–8. https://doi.org/10.1016/j.ejrad.2020.109357.
[28] Fang J, Zhang D, Wilcox C, Heidinger B, Raptopoulos V, Brook A, et al. Metal implants on CT: comparison of iterative reconstruction algorithms for reduction of metal artifacts with single energy and spectral CT scanning in a phantom model. Abdom Radiol 2017;42:742–8. https://doi.org/10.1007/s00261-016-1023-1.
[29] Katsura M, Sato J, Akahane M, Kunimatsu A, Abe O. Current and novel techniques for metal artifact reduction at CT: Practical guide for radiologists. Radiographics 2018;38:450–61. https://doi.org/10.1148/rg.2018170102.
[30] Sharma A, Grieco TF, Zingde SM, Dennis DA, Anderle MR, Komistek RD. In vivo three-dimensional patellar mechanics: Normal knees compared with domed and anatomic patellar components. J Bone Jt Surg - Am Vol 2017;99:e18(1)-e18(13). https://doi.org/10.2106/JBJS.15.01095.
[31] Akbari Shandiz M, Boulos P, Saevarsson SK, Yoo S, Miller S, Anglin C. Changes in knee kinematics following total knee arthroplasty. Proc Inst Mech Eng Part H J Eng Med 2016;230:265–78. https://doi.org/10.1177/0954411916632491.

[32] Sharma GB, Saevarsson SK, Amiri S, Montgomery S, Ramm H, Lichti DD, et al. Radiological method for measuring patellofemoral tracking and tibiofemoral kinematics before and after total knee replacement. Bone Joint Res 2012;1:263–71. https://doi.org/10.1302/2046-3758.110.2000117.
[33] Ho KCT, Saevarsson SK, Ramm H, Lieck R, Zachow S, Sharma GB, et al. Computed tomography analysis of knee pose and geometry before and after total knee arthroplasty. J Biomech 2012;45:2215–21. https://doi.org/10.1016/j.jbiomech.2012.06.004.
[34] von Eisenhart-Rothe R, Vogl T, Englmeier KH, Graichen H. A new in vivo technique for determination of femoro-tibial and femoro-patellar 3D kinematics in total knee arthroplasty. J Biomech 2007;40:3079–88. https://doi.org/10.1016/j.jbiomech.2007.03.020.
[35] Teel AJ, Esposito JG, Lanting BA, Howard JL, Schemitsch EH. Patellar Resurfacing in Primary Total Knee Arthroplasty: A Meta-Analysis of Randomized Controlled Trials. J Arthroplasty 2019;34:3124–32. https://doi.org/10.1016/j.arth.2019.07.019.
[36] Minnema J, van Eijnatten M, Hendriksen AA, Liberton N, Pelt DM, Batenburg KJ, et al. Segmentation of dental cone-beam CT scans affected by metal artifacts using a mixed-scale dense convolutional neural network. Med Phys 2019;46:5027–35. https://doi.org/10.1002/mp.13793.
[37] Kujala UM, Jaakkola LH, Koskinen SK, Taimela S, Hurme M, Nelimarkka O. Scoring of Patellofemoral Disorders. Arthrosc J Arthrosc Relat Surg 1993;9:15–163. https://doi.org/10.1016/S0749-8063(05)80366-4.
[38] Ummels PEJ, Lenssen AF, Barendrecht M, Beurskens AJHM. Reliability of the Dutch translation of the Kujala Patellofemoral Score Questionnaire. Physiother Res Int 2017;22:e1649. https://doi.org/10.1002/pri.1649.

Appendix 1: Design space exploration for assessing the patellar tracking pattern

In this study, a method for the assessment of the patellar tracking pattern using dynamic CT was developed. This Appendix describes the steps that were taken to design this method, discusses methods that were not sufficient and provides recommendations for future optimisation of the method.

Segmentation

For the assessment of the patellar tracking pattern, accurate segmentations of the bones and implant components were required. Pre TKA, a convolutional neural network was used to automatically segment the femur, patella and tibia in both the static and dynamic scans. Post TKA, this convolutional neural network could not be used to segment the bones. Neither did segmentation techniques that were solely based on thresholding or region growing. This was due to the metal (and motion) artifacts that were present in the (dynamic) post TKA scans. Especially the posterior part of the patella was severely affected by these artifacts. Therefore, it was decided to perform a thresholding operation followed by manual fine-tuning (i.e. with painting, erasing and smoothing) to segment the post TKA bones and implant components. The implant components did not need much manual fine-tuning. However, the patella did require a lot of manual fine-tuning. Segmentation of the patella was therefore the most time-consuming part of the whole segmentation and registration process. Accordingly, future research should focus on automatization of the segmentation process of the patella, for example by using a convolutional neural network that is trained on images with metal (and motion) artifacts. Segmentation based on edge detection of the anterior surface of the patella might also be attempted, as the anterior surface was least affected by metal artifacts.
Considering the time-consuming segmentation process, it was not feasible to segment the bones and implant components in all 41 dynamic CT frames. Therefore, it was decided to select four dynamic CT frames to continue with. The dynamic CT frames with the maximum and minimum tibiofemoral flexion angles were first selected, as this would provide information on the patellar tracking pattern over a maximum trajectory. Subsequently, two dynamic CT frames in between were selected.

Registration

As the segmentations of the post TKA patellae required a lot of manual fine-tuning, it was decided to register these patellae using rigid image registration (instead of rigid point cloud registration). The dynamic CT image was the fixed image, the static CT image was the moving image and the fixed image was masked with the segmentation of the patella of the dynamic image. Despite adjustments of the registration parameters, this did not provide a good registration. Masking the fixed image with a dilated version of the segmentation of the patella of the dynamic image also did not suffice. Therefore, it was decided to use an initial transform. This initial transform was the result of a binary mask registration, where the segmentation of the dynamic patella was the fixed image, the segmentation of the static patella was the moving image and the fixed image was masked with a dilated segmentation of the dynamic patella. Image registration was then

performed with the result of the binary mask registration as an initial transform, the dynamic CT image as the fixed image and the static CT image as the moving image. The fixed image was masked with a dilated version of the segmentation of the patella of the dynamic image. However, this still did not provide a good registration. Therefore, the transformed static patella segmentation, that resulted from the binary mask registration, was multiplied with the dynamic patella segmentation. The results was then dilated and used to mask the fixed image. Together with some adjustments in the transformation parameter file, this finally resulted in a sufficient registration of the post TKA static and dynamic patellae. The result was sufficient as the anterior surfaces showed a good overlap. The transformation parameters that were used for the binary mask registration are shown in Appendix 4. The transformation parameters that were used for the image registration are shown in Appendix 5. It should be noted that a very small step length and only one resolution were used for the image registration. For larger step lengths and more resolutions, the registration result worsened.
All other registrations were carried out with rigid point cloud registration. The Coherent Point Drift (CPD) algorithm [20] was used, as it did not rely on an initial transform estimate. A disadvantage of the CPD algorithm is that it is relatively slow. A different registration algorithm might therefore be preferred when all dynamic frames are to be analysed.

Patellar motion analysis

For the patellar motion analysis, the anatomical coordinate system of the human knee as proposed by Miranda et al. [23] was chosen as it was the conventional anatomical coordinate system that was used in our department to describe knee kinematics. The choice for Euler angles resulted from the fact that this immediately provided the three angles that we were interested in (i.e. patellar tilt, shift and rotation).

Appendix 2: Qualitative and quantitative image analysis results

Table A: Qualitative image analysis results of the influence of tube voltage, tube current and reconstruction technique on the visibility of the bones and implant components and on the presence of metal and motion artifacts for the static CT scans.

	Q1	Q2	Q3	Q4	Q5	Q6
100 kV 10 mAs non-SEMAR soft tissue	2	3	4	2	3	2
120 kV 10 mAs non-SEMAR soft tissue	4	4	5	4	4	3
120 kV 40 mAs non-SEMAR soft tissue	4	4	5	4	4	3
120 kV 150 mAs non-SEMAR soft tissue	4	3	4	4	5	3
100 kV 10 mAs SEMAR soft tissue	3	2	5	4	4	3
120 kV 10 mAs SEMAR soft tissue	3	3	4	3	3	2
120 kV 40 mAs SEMAR soft tissue	3	3	3	3	4	3
120 kV 150 mAs SEMAR soft tissue	3	3	3	3	4	3
100 kV 10 mAs non-SEMAR bone	2	3	4	2	3	2
120 kV 10 mAs non-SEMAR bone	2	2	4	2	3	2
120 kV 40 mAs non-SEMAR bone	3	3	4	3	4	2
120 kV 150 mAs non-SEMAR bone	5	5	5	4	5	4
100 kV 10 mAs SEMAR bone	3	3	4	3	3	2
120 kV 10 mAs SEMAR bone	3	3	3	2	3	2
120 kV 40 mAs SEMAR bone	3	4	4	4	4	4
120 kV 150 mAs SEMAR bone	3	4	5	4	4	3

Table B: Qualitative image analysis results of the influence of CT imaging parameters on the visibility of the bones and implant components and on the presence of metal and motion artifacts for the dynamic CT scans.

	Q1	Q2	Q3	Q4	Q5	Q6
100 kV 7 mAs non-SEMAR soft tissue	2	1	3	2	2	2
120 kV 7 mAs non-SEMAR soft tissue	2	2	3	3	3	2
120 kV 14 mAs non-SEMAR soft tissue	3	3	3	3	3	2
100 kV 7 mAs SEMAR soft tissue	1	1	2	1	2	1
120 kV 7 mAs SEMAR soft tissue	2	1	2	2	3	1
120 kV 14 mAs SEMAR soft tissue	2	1	2	1	2	1
100 kV 7 mAs non-SEMAR bone	2	2	3	2	2	1
120 kV 7 mAs non-SEMAR bone	3	3	3	2	2	1
120 kV 14 mAs non-SEMAR bone	1	2	3	2	2	2
100 kV 7 mAs SEMAR bone	1	1	2	2	2	1
120 kV 7 mAs SEMAR bone	1	1	2	2	2	1
120 kV 14 mAs SEMAR bone	2	2	2	2	2	1

Table C: Qualitative image analysis results of the influence of the implant material on the visibility of the bones and implant components and on the presence of metal and motion artifacts.

	Q1	Q2	Q4	Q6
CoCr implant frame 1	4	4	4	4
CoCr implant frame 2	4	4	4	4
CoCr implant frame 3	3	4	4	3
Zr implant frame 1	3	3	2	2
Zr implant frame 2	3	3	3	2
Zr implant frame 3	3	3	3	3

Table D: Quantitative image analysis results of the influence of tube voltage, tube current and reconstruction technique on static CT image quality.

	HU mean	Image noise	SNR
100 kV 10 mAs non-SEMAR soft tissue	259.37	376.03	0.69
120 kV 10 mAs non-SEMAR soft tissue	199.48	347.89	0.57
120 kV 40 mAs non-SEMAR soft tissue	199.03	346.99	0.57
120 kV 150 mAs non-SEMAR soft tissue	179.16	351.62	0.51
100 kV 10 mAs SEMAR soft tissue	980.35	697.53	1.41
120 kV 10 mAs SEMAR soft tissue	782.51	538.46	1.45
120 kV 40 mAs SEMAR soft tissue	761.22	508.08	1.50
120 kV 150 mAs SEMAR soft tissue	752.81	527.17	1.43
100 kV 10 mAs non-SEMAR bone	192.92	408.18	0.47
120 kV 10 mAs non-SEMAR bone	174.62	383.73	0.46
120 kV 40 mAs non-SEMAR bone	206.83	375.91	0.55
120 kV 150 mAs non-SEMAR bone	180.76	379.27	0.48
100 kV 10 mAs SEMAR bone	836.35	624.96	1.34
120 kV 10 mAs SEMAR bone	720.67	516.41	1.40
120 kV 40 mAs SEMAR bone	706.98	502.67	1.41
120 kV 150 mAs SEMAR bone	696.17	516.30	1.35

Appendix 3: Cadaveric patellar tracking pattern pre versus post TKA

This Appendix provides the differences in the patellar tracking patterns pre versus post TKA of the cadaveric knee. However, it should be noted that the observed patellar tracking patterns do not represent the actual patellar tracking patterns in a patient. This is due to the absence of quadriceps muscle activation and to the implantation of a left femoral component in a right knee.

The pre and post TKA patellar flexion, tilt, rotation and shift at the four different tibiofemoral flexion angles are shown in Figure 6. Both pre and post TKA, the patellar flexion angle increased with an increasing tibiofemoral flexion angle. The post TKA patellar flexion angle was always higher than the pre TKA patellar flexion angle, with a maximum difference of about 20° which was observed at about 10° of knee flexion. Both pre and post TKA, the patellar tilt was medially oriented in the first degrees of tibiofemoral flexion and became laterally oriented after about 30° of knee flexion pre TKA and after about 15° of knee flexion post TKA. Pre TKA, the patella continued to tilt more laterally with an increasing tibiofemoral flexion angle. Post TKA, the patella also tilted more laterally with an increasing tibiofemoral flexion angle, but after 42° of tibiofemoral flexion, the patella tilted slightly less laterally. For knee flexion angles greater than 10°, the patellar tilt was always higher post TKA than pre TKA with a maximum difference of about 6° at a knee flexion angle of about 40°. Both pre and post TKA, patellar rotation was always medially oriented. Pre TKA, the patella rotated slightly more laterally in the first 25° of knee flexion and then rotated more medially with an increasing knee flexion angle. Post TKA, the patella rotated slightly more medially until 15° of knee flexion and then rotated more laterally with an increasing knee flexion angle. For tibiofemoral flexion angles greater than 25°, patellar rotation was more lateral post TKA than pre TKA, with a maximum difference of about 3° at a knee flexion angle of about 55°. Both pre and post TKA, the patellar shift was lateral for all knee flexion angles. Pre TKA, the patella shifted more laterally with an increasing knee flexion angle. Post TKA, the patellar shift was almost constant. Patellar shift was slightly more lateral post TKA than pre TKA for knee flexion angles until 30° and then became slightly more medial. However, the maximum difference in patellar shift pre versus post TKA was less than 1.5 mm. This maximum difference was observed at the first degrees of knee flexion.

To visualize the patellar tracking pattern pre and post TKA, a projection of the origin of the patellar anatomical reference frame along the patellar AP axis on the (native or implant) femoral trochlea is depicted in Figure 7 for each of the four tibiofemoral flexion angles. Pre TKA, the patella entered the femoral trochlea from medially and then moved laterally with an increasing knee flexion angle. Post TKA, the patella entered the groove in the femoral component from laterally and then roughly remained at the same mediolateral position while the knee flexion angle increased.

Appendix 4: Transform parameter file for binary mask registration

```
// **********************
// * rigid
// **********************

// **********************
// * ImageTypes
// **********************
(FixedInternalImagePixelType "float")
(MovingInternalImagePixelType "float")
(UseDirectionCosines "true")

// **********************
// * Components
// **********************
(Registration "MultiResolutionRegistration")
(FixedImagePyramid "FixedSmoothingImagePyramid")
(MovingImagePyramid "MovingSmoothingImagePyramid")
(Interpolator "NearestNeighborInterpolator")
(ResampleInterpolator "FinalNearestNeighborInterpolator")
(Metric "AdvancedMeanSquares")
(Resampler "DefaultResampler")
(Optimizer "AdaptiveStochasticGradientDescent")
(Transform "EulerTransform")

// **********************
// * Mask settings
// **********************
(ErodeMask "false")

// **********************
// * Optimizer settings
// **********************
(NumberOfResolutions 4)
(MaximumNumberOfIterations 250)
(ASGDParameterEstimationMethod "DisplacementDistribution")
(AutomaticParameterEstimation "true")
(AutomaticTransformInitialization "true")
(AutomaticTransformInitializationMethod "CenterOfGravity")
(Scales 10000.0 10000.0 10000.0 1.0 1.0 1.0)

// **********************
// * Pyramid settings
// **********************
(NumberOfHistogramBins 32)

// **********************
// * Sampler parameters
// **********************
(NumberOfSpatialSamples 2500)
(ImageSampler "RandomCoordinate")
(CheckNumberOfSamples "true")
(NewSamplesEveryIteration "true")
(MaximumNumberOfSamplingAttempts 5)

// **********************
// * Output settings
// **********************
(DefaultPixelValue 0)
(WriteTransformParametersEachIteration "false")
(WriteTransformParametersEachResolution "false")
(WriteResultImage "true")
(ResultImageFormat "mha")
(ResultImagePixelType "float")
```

Appendix 5: Transform parameter file for image registration

```
// **********************
// * rigid
// **********************

// **********************
// * ImageTypes
// **********************
(FixedInternalImagePixelType "float")
(MovingInternalImagePixelType "float")
(UseDirectionCosines "true")

// **********************
// * Components
// **********************
(Registration "MultiResolutionRegistration")
(FixedImagePyramid "FixedSmoothingImagePyramid")
(MovingImagePyramid "MovingSmoothingImagePyramid")
(Interpolator "BSplineInterpolator")
(ResampleInterpolator "FinalBSplineInterpolator")
(Metric "AdvancedMattesMutualInformation")
(BSplineInterpolationOrder 1)
(Resampler "DefaultResampler")
(Optimizer "AdaptiveStochasticGradientDescent")
(Transform "EulerTransform")

// **********************
// * Mask settings
// **********************
 (ErodeMask "true")

// **********************
// * Optimizer settings
// **********************
(NumberOfResolutions 1)
(MaximumNumberOfIterations 500)
(ASGDParameterEstimationMethod "DisplacementDistribution")
(AutomaticParameterEstimation "true")
(MaximumStepLength 0.001)
(AutomaticTransformInitialization "false")
(AutomaticScalesEstimation "true")

// **********************
// * Transform settings
// **********************
(HowToCombineTransforms "Compose")

// **********************
// * Pyramid settings
// **********************
(NumberOfHistogramBins 32)

// **********************
// * Sampler parameters
// **********************
(NumberOfSpatialSamples 5000)
(ImageSampler "RandomCoordinate")
(CheckNumberOfSamples "true")
(NewSamplesEveryIteration "true")
(MaximumNumberOfSamplingAttempts 5)
(FinalBSplineInterpolationOrder 3)

// **********************
// * Output settings
// **********************
(DefaultPixelValue -2048)
(WriteTransformParametersEachIteration "false")
(WriteResultImageAfterEachResolution "true")
(WriteResultImage "true")
(ResultImageFormat "mha")
(ResultImagePixelType "float")
```